nature geoscience

SUPPLEMENTARY INFORMATION

https://doi.org/10.1038/s41561-019-0320-z

In the format provided by the authors and unedited.

Methanogenesis sustained by sulfide weathering during the Great Oxidation Event

Shui-Jiong Wang[1]*, Roberta L. Rudnick[2,3,4], Richard M. Gaschnig[5], Hao Wang[6] and Laura E. Wasylenki[7,8]

[1]State Key Laboratory of Geological Processes and Mineral Resources, China University of Geosciences, Beijing, China. [2]Department of Earth Science, University of California, Santa Barbara, CA, USA. [3]Earth Research Institute, University of California, Santa Barbara, CA, USA. [4]Department of Geology, University of Maryland, College Park, MD, USA. [5]Department of Environmental, Earth and Atmospheric Sciences, University of Massachusetts Lowell, Lowell, MA, USA. [6]State Key Laboratory of Lithospheric Evolution, Institute of Geology and Geophysics, Chinese Academy of Sciences, Beijing, China. [7]School of Earth and Sustainability, Northern Arizona University, Flagstaff, AZ, USA. [8]Department of Chemistry and Biochemistry, Northern Arizona University, Flagstaff, AZ, USA. *e-mail: wsj@cugb.edu.cn

Methanogenesis sustained by sulfide weathering during the Great Oxidation Event

Shui-Jiong Wang[1*], Roberta L Rudnick[2,3], Richard M Gaschnig[4], Hao Wang[5], Laura E Wasylenki[6]

[1] State Key Laboratory of Geological Processes and Mineral Resources, China University of Geosciences, Beijing 100083, China

[2] Department of Earth Science and Earth Research Institute, University of California, Santa Barbara, CA 93106 USA

[3] Department of Geology, University of Maryland, College Park, MD 20742 USA

[4] Department of Environmental, Earth & Atmospheric Sciences, University of Massachusetts Lowell, MA, 01854 USA

[5] State Key Laboratory of Lithospheric Evolution, Institute of Geology and Geophysics, Chinese Academy of Sciences, Beijing, 100029, China

[6] School of Earth and Sustainability and Dept. of Chemistry & Biochemistry, Northern Arizona University, Flagstaff, AZ 86011 USA

Supplementary Material

Supplementary Section 1

The fidelity of diamictite composites as proxies of UCC Ni isotope composition

Glacial sediments provide a robust estimate of the average composition of the upper continental crust (UCC), because large glaciers and ice sheets mechanically erode and mix the terranes they traverse, with little evidence for chemical weathering associated with transport and deposition. This approach was first utilized by Goldschmidt[1], and later studies added credence to this approach[2-5].

Gaschnig et al.[3] collected about 150 glacial diamictite samples deposited in four broad geological intervals (*i.e.*, Mesoarchean, Paleoproterozoic, Neoproterozoic, and Paleozoic) from four modern continents. Information on stratigraphic units, ages, and localities appeared in previous publications[3,4] and is summarized in Supplementary Table S1. The ~150 individual diamictites cover 27 stratigraphic units. Twenty-four composites were made by thoroughly mixing equal weights of powder from each individual sample of a stratigraphic unit[4]. These diamictite composites were intended to serve as a new reference suite of upper crustal samples, analogous to PAAS (post-Archean Australian shale)[6] and NASC (North American shale composite)[7], representing the average compositions of the glacially sampled upper crust in each stratigraphic unit or time period[4].

Neither post-depositional processes nor local provenance likely influence the Ni isotopic systematics in the diamictite composites. The absence of development of paleosols in any of the sampled deposits suggest that syn- or post-depositional

39 modifications are negligible[3-5]. The chemical weathering signatures that are preserved
40 in all diamictites are interpreted to be inherited from the sources[3,5]. Even the isotope
41 ratios of Li, a relatively mobile element during weathering and low-grade metamorphic
42 processes[8], are argued in these samples to represent source signatures, because of the
43 lack of systematic changes in δ^7Li along vertical profiles within the diamictite units[5].
44 Nickel is less mobile than Li during post-depositional processes[9], and thus the Ni
45 isotopic compositions of the diamictite composites were very likely inherited from the
46 UCC over which the glaciers traversed. Local provenance affects some major elements,
47 but not Ni or other transition metals[3,4]. For example, the Neoproterozoic Chuos and
48 Ghuab formations in Namibia contain significantly high CaO contents, reflecting a
49 large carbonate component in their provenances. The Mesoarchean Mozaan Group and
50 Paleoproterozoic Makganyene formation have relatively high total Fe contents, likely
51 due to the presence of iron formations in their source areas. However, their transition
52 metal signatures are similar to other diamictites of the same ages, which are interpreted
53 as global signatures[4]. As documented in previous studies[3,4], the Paleozoic Dwyka West
54 diamictites, which derive from >2.0 Ga crustal sources, have transitional metal
55 signatures mirroring the Mesoarchean diamictite composites (Fig. 3 of Ref *4*). Thus,
56 the Ni isotope systematics of this composite likely reflect a Mesoarchean UCC
57 signature. Other than this one example, provenance does not exert a control on the Ni
58 isotopic systematics of the diamictite composites, which is further supported by the
59 absence of any correlation between $\delta^{60/58}$Ni values and provenance indicators
60 (Supplementary Fig. S1). Consequently, we conclude that the diamictite composites

provide a robust average Ni isotopic composition of the contemporaneous UCC.

Supplementary Section 2

The significance of the difference in Ni isotope composition between 2.9 Ga and 2.4-2.2 Ga composites

The Ni isotope compositions of the composites are presented in Supplementary Table S2. The difference in Ni isotope compositions between Mesoarchean and Paleoproterozoic diamictite composites is quantified using two-tail Student *t*-tests (Supplementary Table S3). Before the *t*-test, the hypothesis of equal variance between the two populations was evaluated with an *F* test. The *F* value is lower than the *F* critical value (1.1 vs. 9.0), so we applied the *t*-test assuming equal variances. As shown in Supplementary Table S3, the Ni isotopic difference between Mesoarchean and Paleoproterozoic diamictites is significant (p = 0.03). Among the Paleoproterozoic composites, the youngest composite from the Timeball Hill formation was deposited after the GOE under oxic conditions during which red-beds were well developed, whereas the others were not. Because we are more interested in the isotopic shift before the appearance of well-developed red-beds, we excluded the Timeball Hill diamictite composite in a separate *t*-test run. The results showed an even more significant difference between Mesoarchean and Paleoproterozoic composites (p = 0.009).

Nearly all of the Mesoarchean diamictite composites have $\delta^{60/58}$Ni values lighter than the average of igneous lithologies in Supplementary Fig. S2. We note that these igneous rocks are essentially sulfide-barren, such that their tight average of +0.13 ± 0.13‰ likely represents only the silicate portion of the Mesoarchean and

Paleoproterozoic UCC. The diamictites, whose total S contents are slightly higher, are likely isotopically lighter due to the presence of a small proportion of isotopically light, sulfide-hosted Ni.

Supplementary Section 3

Isotope mass balance model

To compare the contributions of sulfide weathering to the total Ni weathering flux before and during the GOE, we applied an isotopic mass balance model. First, we consider the Ni weathering flux at any time point to consist of two components: Ni from sulfide weathering (f) and Ni from silicate weathering ($1-f$):

$$\delta^{60/58}Ni_{weathering} = f \times \delta^{60/58}Ni_{sulfide} + (1-f) \times \delta^{60/58}Ni_{silicate}. \quad (1)$$

We assume that f would have been quite small during Mesoarchean anoxic weathering, but increased with the onset of oxidative weathering.

Oxidative dissolution of sulfides in acidified surface waters (pH < 4.5) during the GOE[10] likely released all sulfide-bound Ni to solutions wholesale, without driving significant Ni isotope fractionations. A recent experimental study also found that there is a lack of Ni isotope fractionation during silicate dissolution[11]. Therefore, the change in the contribution of sulfide-derived Ni to the total Ni weathering flux between the Mesoarchean (time point 1) and Paleoproterozoic (time point 2) can be expressed as follows:

$$\Delta f = f_2 - f_1 = (\delta^{60/58}Ni_{weathering2} - \delta^{60/58}Ni_{weathering1})/(\delta^{60/58}Ni_{sulfide} - \delta^{60/58}Ni_{silicate}), \quad (2)$$

where the isotope value of the Ni weathering flux ($\delta^{60/58}Ni_{weathering}$) is a function of the

fraction of all UCC Ni removed by chemical weathering (F), and the Ni isotope value of the remaining UCC Ni ($\delta^{60}Ni_{UCC}$) is computed according to the expression:

$$F \times \delta^{60/58}Ni_{weathering} + (1\text{-}F) \times \delta^{60/58}Ni_{UCC} = \delta^{60/58}Ni_{UCC\text{-}unweathered} \quad (3)$$

In the model calculations, because we do not know the isotopic composition of the unweathered UCC, the $\delta^{60/58}Ni$ value of the unweathered UCC ($\delta^{60/58}Ni_{UCC\text{-}unweathered}$) is assumed to be similar to sulfide-barren igneous rocks, +0.13‰ (Supplementary Fig. S3). The exact value chosen is of no consequence to our constraints on Δf, which is what we aim to constrain. The $\delta^{60/58}Ni$ value of the weathered residue of the UCC ($\delta^{60/58}Ni_{UCC}$) at different age points is represented by the average values determined for the diamictite composites. We use the maximum Ni isotope fractionation observed between sulfides and silicates ($\delta^{60/58}Ni_{sulfide}$ - $\delta^{60/58}Ni_{silicate}$) of -1.5‰ (see Supplementary Fig. S3), because this leads to minimum values of Δf.

Therefore, the proportional change in contribution of sulfide weathering to Ni flux during the GOE (Δf) can be expressed as a function of F_1 and F_2:

$$\Delta f = \{[0.13\text{-}(1\text{-}F_2) \times \delta^{60/58}Ni_{UCC2}]/F_2 - [0.13\text{-}(1\text{-}F_1) \times \delta^{60/58}Ni_{UCC1}]/F_1\}/(\delta^{60/58}Ni_{sulfide} - \delta^{60/58}Ni_{silicate})$$

The values of F_1 and F_2 are poorly constrained, as is their ratio, F_2/F_1, which compares the fractions of all Ni removed from the UCC by chemical weathering during and before the GOE. One recent study has shown that there is no significant change in weathering intensity from Mesoarchean to across the GOE[12], which corresponds to $F_2/F_1 = 1$. It is rather unlikely that the fraction of Ni removed from the crust decreased when oxidative weathering began, so 1 is likely a minimum for F_2/F_1. In our calculations, we vary the F_2/F_1 over the range of 1.0-1.5. The results are shown in

Supplementary Fig. S4. Another parameter that is not well constrained is the fraction of Ni removed during chemical weathering (F_1 or F_2). Given that Ni is generally insoluble during chemical weathering[13], we tentatively assumed F to be less than 0.1 in our modeling. Resulting computations show that the fraction of sulfide-derived Ni in total weathering flux during the GOE likely have increased by at least 30% and quite possibly much more, possibly dominating the Ni flux during the heart of the GOE (Supplementary Fig. S4 and S5). Given the uncertainties of parameters such as F and F_2/F_1 ratio, in the modelling, we acknowledge that tight constraining the contribution of sulfide weathering during the GOE apparently needs additional proxies, but this calculation gives a first-order estimate of how long enhanced input of sulfide-derived Ni may have lasted, and highlights the importance of sulfide weathering in terrestrial Ni cycle during the GOE.

Supplementary Section 4

Supplementary Table S1. Information for glacial diamictite composites.

Composite name	Stratigraphic unit	Country (State/province)	Age (Ga)	Individual sample number
Mozaan	Mozaan Grp.	S. Africa	2.9	7
Afrikander	Afrikander Frm.	S. Africa	2.9	4
Promise	Promise Frm.	S. Africa	2.9	3
Coronation	Coranation Frm.	S. Africa	2.9	5
Duitschland	Duitschland Frm.	S. Africa	2.4	5
Timeball Hill	Timeball Hill Frm.	S. Africa	2.2	6
Makganyene	Makganyene Frm.	S. Africa	2.4	6
Ramsay Lake	Ramsay Lake Frm.	Canada	2.4	5
Bruce	Bruce Frm.	Canada	2.4	3
Gowganda	Gowganda Frm.	Canada	2.4	16
Bottle Creek	Bottle Creek Frm.	USA	2.4	4
Gaskiers	Gaskiers Frm.	Canada	0.58	4
Pocatello	Pocatello Frm.	USA	0.7	6
Konnarock	Konnarock Frm.	USA	0.7	8
Nantuo	Nantuo Frm.	China	0.64	13
Gucheng	Gucheng Frm.	China	0.7	5
Blaubeker	Blaubeker Frm.	Namibia	0.7	6
Kaigas	Kaigas Frm.	Namibia	0.75	5
Chuos	Chuos Frm.	Namibia	0.7	5
Numees	Numees Frm.	Namibia	0.6	8
Ghaub	Ghaub Frm.	Namibia	0.64	3
Bolivian	Machareti + Mandiyuti Grps	Bolivia	0.3	6
Dwyka West	Dwyka Grp.	S. Africa	0.3	8
Dwyka East	Dwyka Grp.	S. Africa + Namibia	0.3	8

Modified after Refs (3) and (4). The absolute age and the correlation to other glacial units for the Bottle Creek diamictite composite from Wyoming are unknown, but it is roughly correlated to between Ramsay Lake and Bruce formation.

Supplementary Table S2. Ni isotopic compositions and total sulfur contents of the diamictite composites, TTGs, komatiite, and USGS standards.

Sample	Age (Ga)	$^{60}Ni_{SRM986}$ (‰)	2SD	Ni[a] (ppm)	TS[b] (wt%)
Diamictites					
Mozaan	2.9	0.04	0.09	141	0.258
Afrikander		0.09	0.03	227	
Afrikander*		0.10	0.03		
average	2.9	0.09	0.02		0.034
Promise	2.9	-0.01	0.05	152	0.174
Coronation	2.9	0.07	0.09	114	0.238
Duitschland	2.4	0.19	0.06	61.3	0.003
Timeball Hill		0.04	0.08	38.7	
Timeball Hill*		0.05	0.04		
average	2.2	0.04	0.02		0.008
Makganyene	2.4	0.11	0.05	37.3	0.217
Ramsay Lake	2.4	0.11	0.07	39.7	0.104
Bruce	2.4	0.20	0.04	32.4	0.031
Gowganda	2.4	0.14	0.03	55.9	0.078
Bottle Creek	2.4	0.10	0.05	37.8	0.004
Gaskiers	0.58	0.26	0.05	11.4	0.054
Pocatello	0.7	0.02	0.05	25.9	0.005
Konnarock	0.7	0.11	0.04	21.9	0.001
Nantuo	0.64	0.16	0.09	28.8	0.004
Gucheng	0.7	0.05	0.06	34.9	0.001
Blaubeker	0.7	0.13	0.09	14.1	0.001
Kaigas	0.75	0.10	0.03	29.5	0.000
Chuos	0.7	0.04	0.07	29.5	0.003
Numees	0.6	-0.02	0.04	16	0.002
Ghaub	0.64	0.14	0.05	17.4	0.000
Bolivian	0.3	0.09	0.05	18.4	0.021

Dwyka West	0.3	-0.07	0.06	79.9	0.229
Dwyka East	0.30	0.14	0.06	32.5	0.025
TTGs					
14SA01_Kaap Valley	3.23	0.11	0.03	16.8	
14SA31_Theespruit	3.46	0.17	0.02	31.2	
Komatiites					
SC5_Komati	3.48	0.10	0.10	2696	0.054
SC7_Komati	3.48	0.16	0.02	847	0.021
SC9_Komati	3.48	0.11	0.07	1947	0.022
SC15_Komati	3.48	0.14	0.05	888	0.004
HG5_Hooggenoeg	3.47	0.18	0.05	1156	
HG15_Hooggenoeg	3.47	0.11	0.05	1037	
HG16_Hooggenoeg	3.47	0.07	0.07	1136	
SS1_Sandspruit	3.55	0.02	0.04	1690	
SS5_Sandspruit	3.55	0.09	0.06	1594	
SS6_Sandspruit	3.55	0.13	0.04	1181	
SS8_Sandspruit	3.55	0.20	0.08	1512	
Standards					
Nod-A-1 (n=10)		1.10	0.07		
BIR-1 (n=5)		0.12	0.03		
BHVO-1 (n=4)		0.03	0.03		
SCO-1 (n=5)		0.08	0.07		
SDO-1 (n=4)		0.60	0.05		

[*] Repeat sample dissolution, column chemistry and instrumental analysis; [a] Ni concentrations of the diamictite composites and komatiites are from Refs (*4*) and (14), respectively. Total sulfur contents of the komatiites are from Ref (14).

Supplementary Table S3. Results of statistical *t*-test for comparisons of Mesoarchean and Paleoproterozoic diamictite composites.

	Degree of freedom	Calculated t	Critical t (two-tail)	P
Mesoarchean and Paleoproterozoic composites	9	2.550	2.262	0.0312
Mesoarchean and Paleoproterozoic composites (without Timeball Hill)	8	3.389	2.306	0.0095

Supplementary Section 5

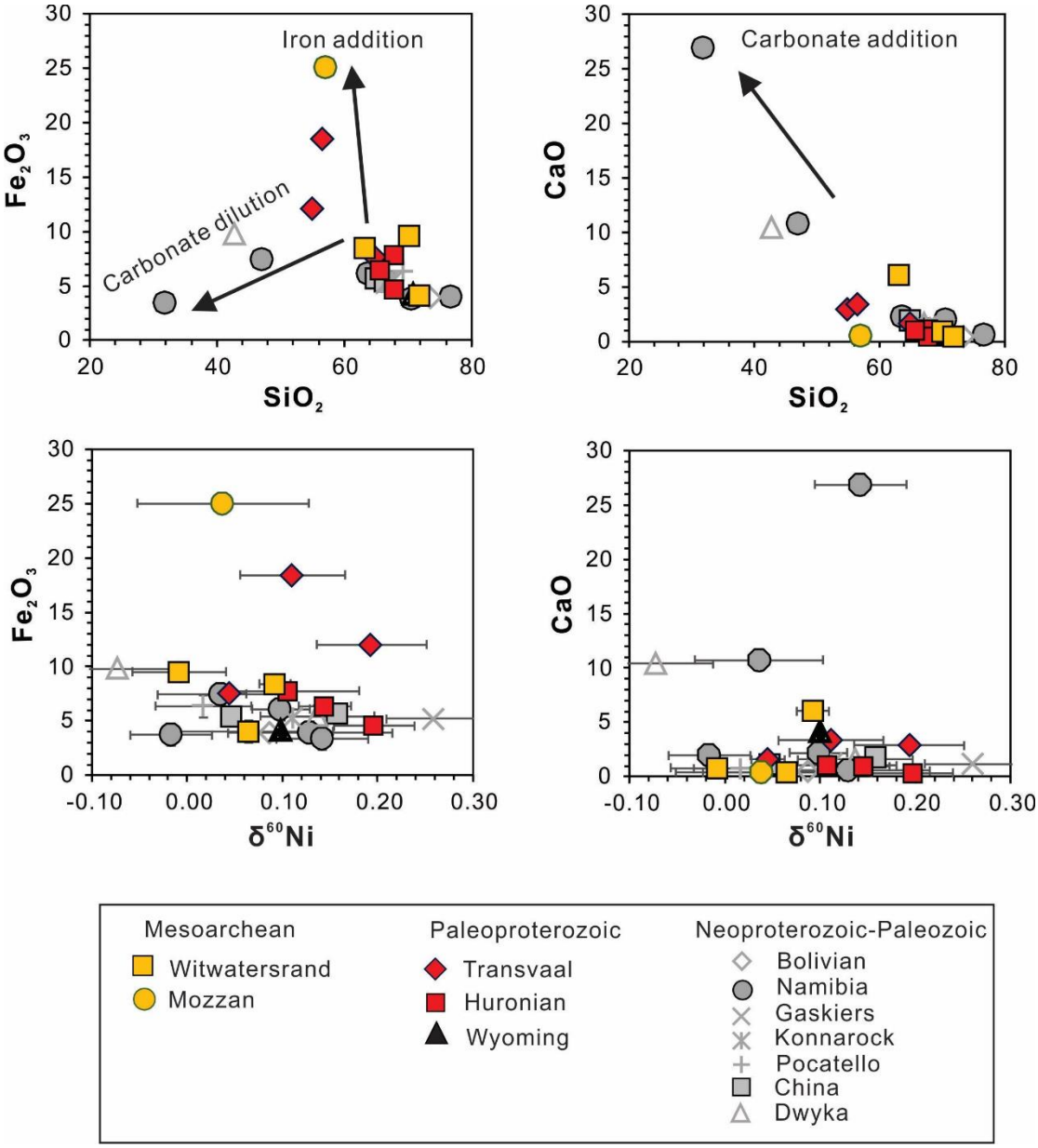

Supplementary Fig. S1. Diagrams showing that Ni isotopic compositions of the diamictite composites are not influenced by provenance. Some diamictites have major elements showing the effects of local provenance (*e.g.*, carbonate and iron formation)[3]; however, the same samples do not show anomalies in Ni isotope compositions compared to others of the same age. The uncertainty of δ^{60}Ni, based on the external rock standards, are better than 0.07‰.

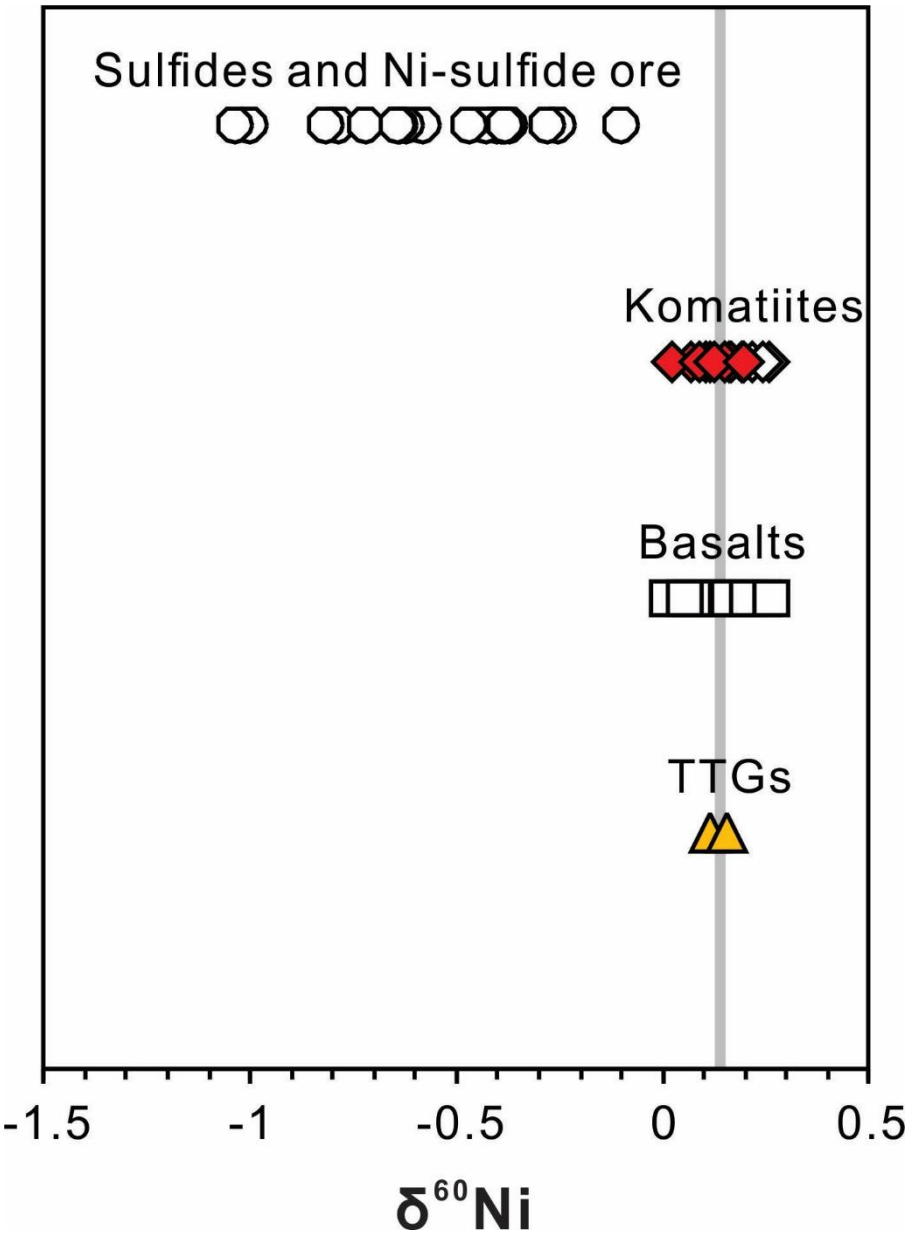

Supplementary Fig. S2. Nickel isotopic compositions of sulfides[15,16], komatiites[17], basalts[15,18-20], and Archean TTGs (this study). The Ni isotope results of Archean komatiites (red diamond) and TTGs (yellow triangle) analyzed in this study are reported in Supplementary Table S2. Note that the igneous samples are very low in total S contents (Table S2), such that their collective average (+0.13 ± 0.13‰; grey, vertical line) likely represents the silicate-only portion of the crust.

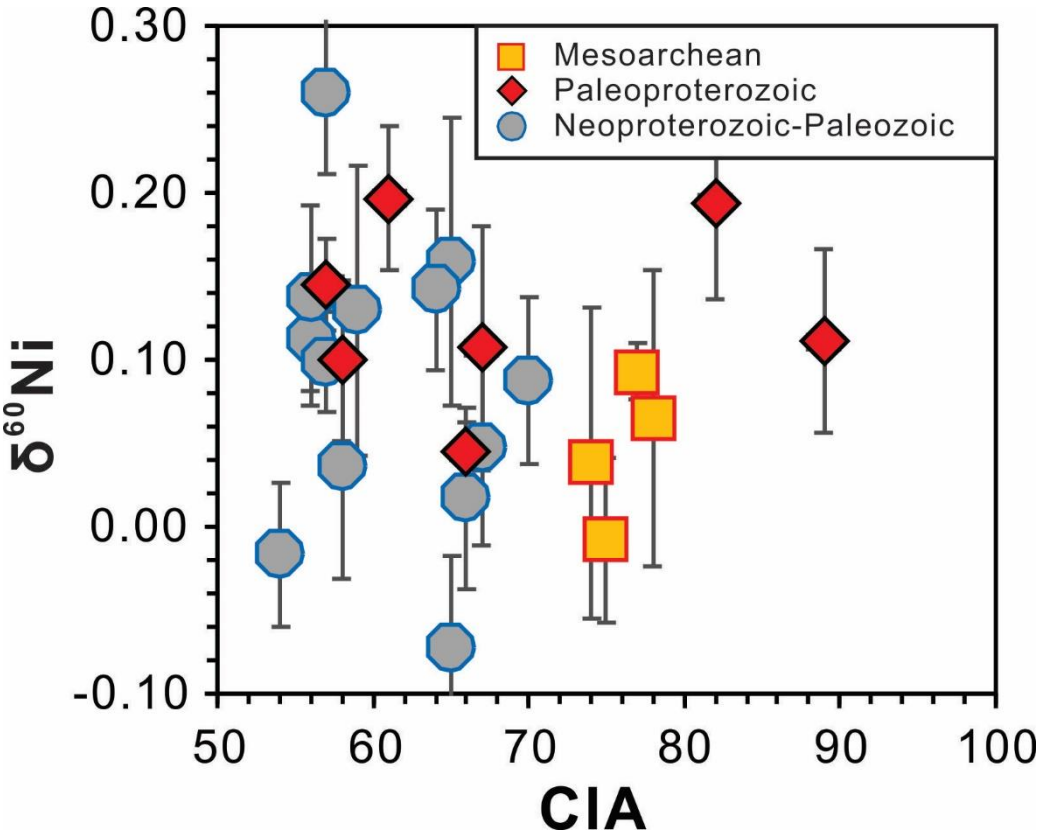

Supplementary Fig. S3. Diamictite composites do not display correlation between δ^{60}Ni and CIA values, suggesting that the Ni isotope compositions of the diamictites are not controlled by weathering intensity but rather a switch of weathering style, *i.e.*, from anoxic weathering to oxidative weathering. The uncertainty of δ^{60}Ni, based on rock standards, is better than 0.07‰.

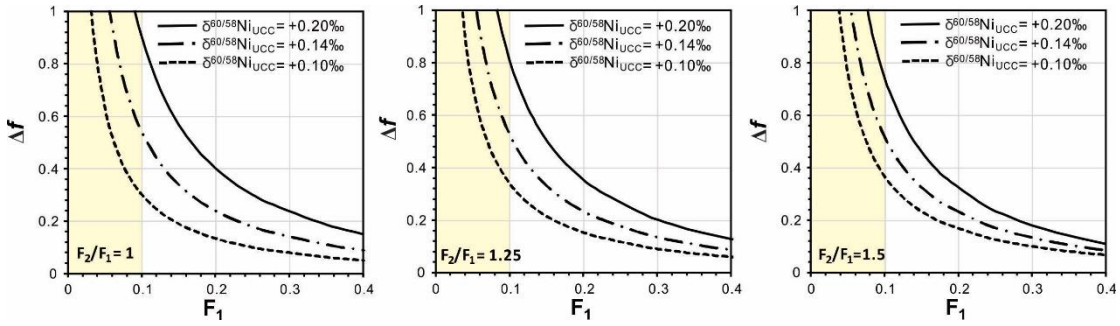

Supplementary Fig. S4. Contribution of sulfide weathering to terrestrial Ni weathering flux as a function of the fraction of Ni weathered from the UCC. The average δ^{60}Ni value of the Mesoarchean diamictite composites (0.05 ± 0.09‰) is taken as the initial Ni isotope composition of the weathered UCC prior to sulfide weathering. See text for discussion of parameterization.

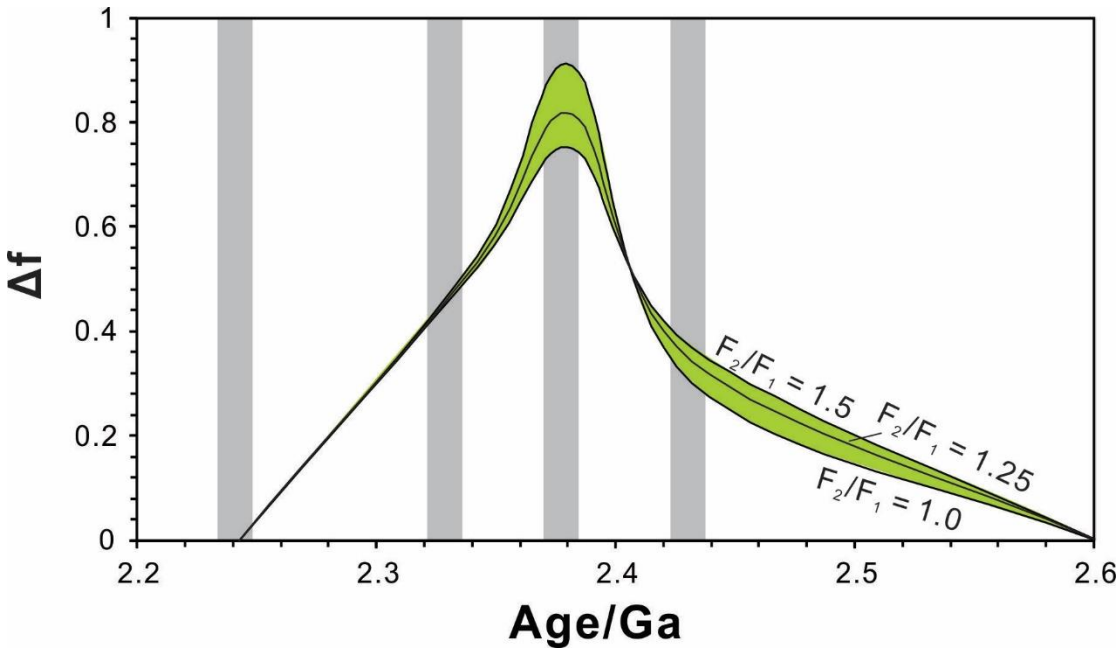

Supplementary Fig. S5. Modelling shows the evolution of the contribution of sulfide weathering to Ni flux during the four glaciations across the GOE (grey bars). The Δf at different glacial events are calculated by assuming the $F_1 = 0.1$ and taking into account the δ^{60}Ni values of the diamictite composites from the four glacial units.

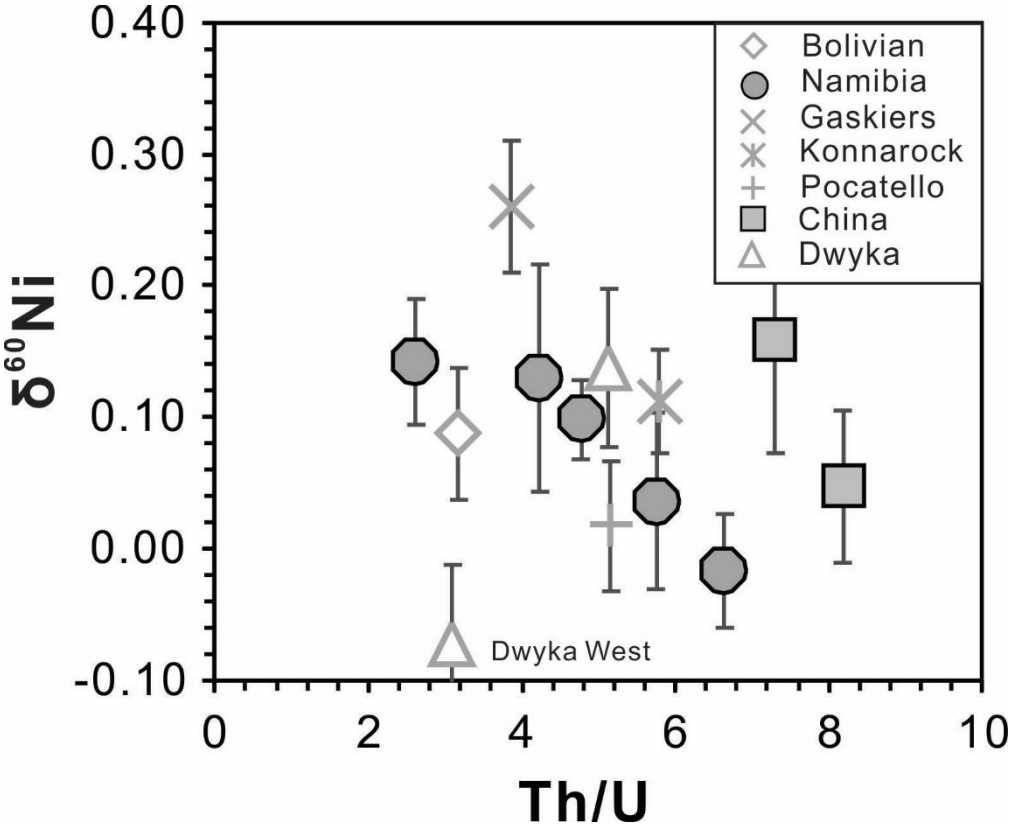

Supplementary Fig. S6. Variation of δ^{60}Ni as a function of Th/U ratio for the Neoproterozoic-Paleozoic diamictite composites. Th/U data are from Gaschnig *et al.*[4]. A weak, negative correlation suggests that the Ni isotopic composition of Neoproterozoic-Paleozoic UCC is influenced by the amount of oxidative weathering. Note that composites from the same locality display strong negative correlation (*e.g.,* Namibia). The Dwyka West diamictite composite was deposited during the Paleozoic but derives from >2.0 Ga crustal sources and mirrors the transitional metal signatures of the Mesoarchean diamictite composites[3,4].

References:

1 Goldschmidt, V. Grundlagen der quantitativen Geochemie. *Fortschr. Mineral. Krist. Petrog* **17**, 12 (1933).

2 Canil, D. & Lacourse, T. An estimate for the bulk composition of juvenile upper continental crust derived from glacial till in the North American Cordillera. *Chem Geol* **284**, 229-239 (2011).

3 Gaschnig, R. M. *et al.* Onset of oxidative weathering of continents recorded in the geochemistry of ancient glacial diamictites. *Earth Planet. Sci. Lett* **408**, 87-99 (2014).

4 Gaschnig, R. M. *et al.* Compositional evolution of the upper continental crust through time, as constrained by ancient glacial diamictites. *Geochim. Cosmochim. Acta* **186**, 316-343 (2016).

5 Li, S., Gaschnig, R. M. & Rudnick, R. L. Insights into chemical weathering of the upper continental crust from the geochemistry of ancient glacial diamictites. *Geochim. Cosmochim. Acta* **176**, 96-117 (2016).

6 Nance, W. B. & Taylor, S. Rare earth element patterns and crustal evolution—I. Australian post-Archean sedimentary rocks. *Geochim. Cosmochim. Acta* **40**, 1539-1551 (1976).

7 Haskin, L. A., Frey, F. A., Schmitt, R. A. & Smith, R. H. Meteoritic, solar and terrestrial rare-earth distributions. *Phys Chem Earth* **7**, 167-321 (1966).

8 Qiu, L., Rudnick, R. L., McDonough, W. F. & Merriman, R. J. Li and δ^7Li in mudrocks from the British Caledonides: metamorphism and source influences.

Geochim. Cosmochim. Acta **73**, 7325-7340 (2009).

9 Merriman, R., Breward, N., Stone, P., Green, K. & Kemp, S. Element mobility and low-grade metamorphism of mudrocks in British Caledonian Basins. British Geological Survey Open Report, OR/09/017 (2009).

10 Konhauser, K. O. *et al.* Aerobic bacterial pyrite oxidation and acid rock drainage during the Great Oxidation Event. *Nature* **478**, 369-373 (2011).

11 Spivak-Birndorf, L. J., Wang, S.-J., Bish, D. L. & Wasylenki, L. E. Nickel isotope fractionation during continental weathering. *Chem Geol* **476**, 316-326 (2017).

12 Hartmann, J., Li, G. & West, A. Running out of gas: Zircon 18O-Hf-U/Pb evidence for Snowball Earth preconditioned by low degassing. *Geochem. Persp. Let.* **4**, 41-46 (2017).

13 Taylor, S. & McLennan, S. The Continental Crust: Its Evolution and Composition. *Lon on: Blackwell* (1985).

14 Maier, W. D. *et al.* Progressive mixing of meteoritic veneer into the early Earth's deep mantle. *Nature* **460**, 620 (2009).

15 Gueguen, B., Rouxel, O., Ponzevera, E., Bekker, A. & Fouquet, Y. Nickel Isotope Variations in Terrestrial Silicate Rocks and Geological Reference Materials Measured by MC‐ICP‐MS. *Geostand Geoanal Res* **37**, 297-317 (2013).

16 Hofmann, A. *et al.* Comparing orthomagmatic and hydrothermal mineralization models for komatiite-hosted nickel deposits in Zimbabwe using multiple-sulfur,

246 iron, and nickel isotope data. *Miner Deposita* **49**, 75-100 (2014).
247 17 Gall, L., Williams, H. M., Halliday, A. N. & Kerr, A. C. Nickel isotopic
248 composition of the mantle. *Geochim. Cosmochim. Acta* **199**, 196-209 (2016).
249 18 Cameron, V., Vance, D., Archer, C. & House, C. H. A biomarker based on the
250 stable isotopes of nickel. *Proc. Natl. Acad. Sci. USA* **106**, 10944-10948 (2009).
251 19 Chernonozhkin, S. M., Goderis, S., Lobo, L., Claeys, P. & Vanhaecke, F.
252 Development of an isolation procedure and MC-ICP-MS measurement protocol
253 for the study of stable isotope ratio variations of nickel. *J Anal Atom Spectrom*
254 **30**, 1518-1530 (2015).
255 20 Gall, L., Williams, H., Siebert, C. & Halliday, A. Determination of mass-
256 dependent variations in nickel isotope compositions using double spiking and
257 MC-ICPMS. *J Anal Atom Spectrom* **27**, 137-145 (2012).
258 21 Sun, S.-S. & McDonough, W.-s. Chemical and isotopic systematics of oceanic
259 basalts: implications for mantle composition and processes. *Geol. Soc. London*
260 *Spec. Publ* **42**, 313-345 (1989).